Journal of Quantitative Spectroscopy & Radiative Transfer 185 (2016) 79–85

Contents lists available at ScienceDirect

Journal of Quantitative Spectroscopy & Radiative Transfer

journal homepage: www.elsevier.com/locate/jqsrt

Measurements of spectral parameters for nitrous oxide near 4.56 μm using a quantum cascade laser

Fei Li, Hui Zeng, Kuanliang Wang, Shaohua Zhang, Xilong Yu *

State Key Laboratory of High Temperature Gas Dynamics, Institute of Mechanics, Chinese Academy of Sciences, Beijing 100190, China

ARTICLE INFO

Article history:
Received 15 April 2016
Received in revised form
19 August 2016
Accepted 21 August 2016
Available online 1 September 2016

Keywords:
Nitrous oxide
Quantum cascade laser
Linestrength
N_2-broadening coefficient
Temperature exponent

ABSTRACT

Line strengths and nitrogen (N_2)-broadening coefficients for six nitrous oxide transitions were measured using a continuous-wave quantum cascade laser (cw-QCL) operating near 4.56 μm. The temperature dependence of the exponent n for the N_2-broadening coefficients was determined over the range 298–800 K using a sapphire-sealed optical cell. Spectral parameters were determined by fitting absorption spectra with multi-peak Voigt profiles. The line strengths for the six transitions are 0–3% larger than those in the HITRAN 2012 database, while the N_2-broadening coefficients at the reference temperature are 2–5% smaller than the HITRAN 2012 values.

1. Introduction

Laser absorption diagnostics using quantum cascade lasers (QCLs) have enabled non-intrusive, real-time, *in situ* measurements of gas temperatures and species concentration under various flow-fields [1–5]. Laser-based measurements depend on accurate spectral parameters for target transitions, including line_strengths, broadening coefficients, and temperature-dependent exponents. Those parameters obtained from spectroscopic databases such as HITRAN [6] and GEISA [7] are mostly derived from quantum-mechanical calculations and lack experiment validations. In particular, the accuracies of the spectral parameters for triatomic molecules such as H_2O and N_2O are questionable. Accurate experimental measurements of H_2O vapor transitions have been reported from fully resolved absorption measurements in the near-IR [8–11].

Nitrous oxide (N_2O, also known as laughing gas) is important to greenhouse issue because it is 300 times more effective than CO_2 with regard to global warming [12]. It is generally produced through industrial fossil-fuel combustion and is used as an energetic oxidizer for chemical reactions at elevated temperatures. In addition, it is widely studied as a rocket propellant for aerospace applications, such as small satellites [13–17]. Laser absorption methods may be used for N_2O quantification in harsh environments, such as that found in combustion engines [5]. Mid-infrared (IR) laser-based sensors provide more sensitive measurements of N_2O relative to those in the near-IR, because the mid-IR line strengths are at least two orders of magnitudes greater [6]. Meanwhile, line-shape broadening and temperature exponents are crucial parameters that should be calibrated experimentally for engine diagnostics under high-pressure and/or high-temperature conditions.

Spectral parameters for N_2O lines between 500 cm^{-1} and 7500 cm^{-1} are presented in HITRAN [6]. Toth has reported much on N_2O spectra: line_strengths over 900–3600 cm^{-1} and self-broadened line widths over 1800–2360 cm^{-1} [18–20], line_strengths over 3515–7800 cm^{-1}, and N_2- and air-broadened line_widths over 1800–4800 cm^{-1} [21]. Line_strength measurements were obtained by Daumont et al. for the 10-μm region [22], over 4300–5200 cm^{-1} [23],

* Corresponding author.
E-mail addresses: lifei@imech.ac.cn (F. Li), zenghui@imech.ac.cn (H. Zeng), wangkuanliang@imech.ac.cn (K. Wang), shzh@imech.ac.cn (S. Zhang), xlyu@imech.ac.cn (X. Yu).

http://dx.doi.org/10.1016/j.jqsrt.2016.08.016
0022-4073/

and over 5400– 11,000 cm^{-1} [24]. Rachet et al. measured line_strengths over 2400–2850 cm^{-1} [25,26]. Absolute intensities of N_2O transitions were measured in the 4-μm and 3-μm regions by Barbe et al. [27]. Line_strengths, N_2-, O_2-, and air-broadening of N_2O were obtained in the 4.5-μm region by Nemtchinov et al. [28], and in the 4-um and 8-μm region by Lacome et al. [29]. Previous studies were performed with a broad-bandwidth Fourier-transform spectrometer at room temperature, and the results were compared with the HITRAN and GEISA databases. Meanwhile, line_strengths near 8 μm [30] and 2 μm were obtained with narrow-line-width diode laser sensors at room temperature. The strongest vibrational band of N_2O is in the 4.5-μm region, which offers great potential for sensitive detection [6]. However, few measurements of spectral parameters have been performed for the ν_3 fundamental band near 4.5 μm. Loewenstein et al. performed preliminary measurements using a tunable diode laser spectrometer at 297 K [31,32], but there is a lack of data for high-temperature conditions.

Here, a narrow-line-width continuous-wave (cw) QCL near 4.56 μm was used to obtain N_2O spectral parameters over the temperature range 298–800 K and the pressure range 2–200 Torr. Line_strengths, broadening coefficients, and temperature-dependent exponents were obtained to verify the HITRAN 2012 [6] and GEISA 2009 [7] molecular spectroscopic databases. The measurements were conducted in a sapphire-sealed optical cell and absorption spectra were fitted with Voigt line-shape profiles.

2. Fundamental spectroscopy

Laser absorption by a molecular transition at frequency ν is expressed by the Beer–Lambert law in Eq. (1) for transmitted intensity I_t through a gas medium of optical path length L (cm) and incident intensity I_0:

$$\frac{I_t}{I_0} = \exp(-PXS_i(T)\phi(\nu-\nu_0)L) \tag{1}$$

where P (atm) is the pressure, X is the mole fraction of the target absorbing species, $S_i(T)$($cm^{-2}atm^{-1}$) is the line strength of the transition at temperature T (K), and $\phi(\nu-\nu_0)$ (cm) is the line shape function at the center wavelength ν_0. The line-shape function is normalized such that $\int_{-\infty}^{+\infty}\phi(\nu-\nu_0)d\nu = 1$ and the integrated absorbance A (cm^{-1}) can be expressed as:

$$A = PX_{abs}S(T)L \tag{2}$$

Given the line strength at the reference temperature $S_i(T_0{=}296\ K)$ and the energy of the lower state for transition E'' (cm^{-1}), the line_strength at an arbitrary temperature $S(T)$ can be calculated by:

$$S(T) = S(T_0)\frac{Q(T_0)}{Q(T)}\left(\frac{T_0}{T}\right)\exp\left[-\frac{hcE''}{k}\left(\frac{1}{T}-\frac{1}{T_0}\right)\right] \times\left[1-\exp\left(\frac{-hc\nu_0}{kT}\right)\right]\left[1-\exp\left(\frac{-hc\nu_0}{kT_0}\right)\right]^{-1} \tag{3}$$

where h is Planck's constant, c is the speed of light, k is Boltzmann's constant, and $Q(T)$ is the partition function of the molecule.

The line-shape function $\phi(\nu-\nu_0)$ is determined by inhomogeneous broadening (or Doppler broadening) and homogeneous broadening (or collisional broadening) [4]. It offers significant information with regard to pressure, gas concentration, and temperature. A brief discussion of the broadening mechanisms is given below.

Doppler broadening is caused by the random thermal motion of the absorbing molecules. The Doppler lineshape function $\phi_D(\nu)$ is described by a Gaussian profile:

$$\phi_D(\nu) = \frac{2}{\Delta\nu_D}\sqrt{\frac{\ln 2}{\pi}}\exp\left\{-4\ln 2\left(\frac{\nu-\nu_0}{\Delta\nu_D}\right)\right\} \tag{4}$$

where $\Delta\nu_D$ (cm^{-1}) is the Doppler full-width at half maximum (FWHM):

$$\Delta\nu_D = \nu_0\sqrt{\frac{8kT\ln 2}{mc^2}} = 7.1623\times10^{-7}\nu_0\sqrt{\frac{T}{M}} \tag{5}$$

where M (g/mol) is the molecular weight.

Pressure_broadening of spectral transitions is caused by binary collisions of the absorbing and non-absorbing species, where the duration of the collisions is assumed to be negligible. The pressure-broadened line shape has a Lorentzian profile:

$$\phi_c = \frac{1}{\pi}\frac{\frac{\Delta\nu_c}{2}}{\left(\nu-\nu_0\right)^2+\left(\frac{\Delta\nu_c}{2}\right)^2} \tag{6}$$

where $\Delta\nu_c$ (cm^{-1}) is the collisional FWHM that is proportional to the pressure:

$$\Delta\nu_c = P\sum_j X_j 2\gamma_j \tag{7}$$

Here, γ_j ($cm^{-1}atm^{-1}$) is the broadening coefficient due to the collisions between perturbing species j and the absorbing species. The temperature dependence of γ_j can be expressed in terms of the temperature exponent n:

$$\gamma_j = \gamma_j(T_0)\left(\frac{T_0}{T}\right)^{n_j} \tag{8}$$

Under most experimental conditions, both mechanisms are usually important and the broadened line_shape, or Voigt profile [3], is a convolution of the Gaussian and Lorentzian line shapes:

$$\phi_V(\nu) = \int_{-\infty}^{+\infty}\phi_D(u)\phi_L(\nu-u)du \tag{9}$$

3. Experimental setup

Measurements were performed on two strong N_2O transitions near 2192.48 cm^{-1} and 2193.54 cm^{-1} and four weak neighboring transitions, belonging to the ν_3 fundamental and a combination band. The center wavelengths and lower-state energies of these transitions in the P-branch are listed in Table 1. Fig. 1 is a simulated absorption spectrum based on parameters from the HITRAN 2012 database and experimental conditions represented here. The peak absorbances range from 0.05–0.6 for a given optical path length, ensuring sufficient absorption in the experiments.

Table 1
Center wavelengths and lower-state energies of the six transitions here [6].

Line	Wavelength ν_0(cm^{-1})	Lower state Energy E''(cm^{-1})	Transition
1	2192.40	748.33	P 19f
2	2192.44	748.03	P 19e
3	2192.48	469.90	P 33e
4	2193.36	732.38	P 18f
5	2193.40	732.11	P 18e
6	2193.54	442.28	P 32e

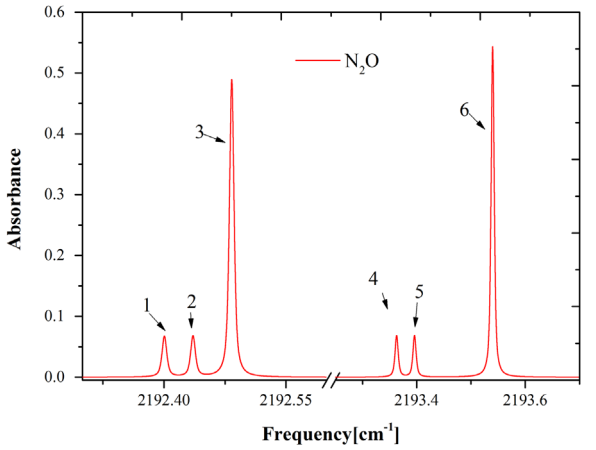

Fig. 1. Simulated N_2O absorption spectra of the target lines and their neighboring features (see Table 1) for $T=298$ K, $P=1.6$ kPa, $X=0.42\%$ and $L=5.86$ cm, using parameters from HITRAN 2012 [6].

A cw distributed-feedback-mode QCL (ALPES LASERS), with a FWHM ≤ 3 MHz, was used to excite the N_2O near 4.56 μm. Previously, a three-section heated static cell was used for the near-IR [8–10,33]. Here, a different optical cell was used for mid-IR measurements; it is similar to those used by Rieker [34] and Rice [35]. Fig. 2 shows a detailed schematic of the cell. A pair of sapphire windows was installed inside a high-temperature resistant tube. The edges of the windows were machined (beveled) with a 45° sealing face so that each window could be mounted with two thin triangle copper seals compressed by a nut. The window faces were wedged to avoid etalon interference. In addition, two 5-cm-long sapphire rods were used to set the 5.86-cm optical path length.

The cell was heated with high-temperature heating tape (OMEGA, STH Series). The temperature of the gas was determined to within 0.75% with a type-K thermocouple (OMEGA) in the center of the cell. Up to 800 K, the cell had a maximum leakage rate of 0.1 Pa min^{-1}. A gas mixture of 0.42% N_2O/N_2 with an uncertainty of 0.5%,filled the heated cell. Gas pressures were measured using 100-torr and 1000-torr 627D MKS Baratron pressure transducers, with accuracies of $\pm 0.12\%$. QCL absorption measurements were conducted when the cell was equilibrated at the set temperature and the pressure were stable. Note that N_2O thermally decomposes above 850 K [36], which was confirmed by appreciable reduction of N_2O absorption. Measurements of spectral parameters were conducted at 10 different temperatures over 298–800 K.

The QCL output was tuned by changing the injection current (controlled by an ILX Lightwave LDX-3232) and the temperature of the laser chip (controlled by an Alpes Lasers TC-3). The laser wavelength was scanned over the entire absorption feature of the target transitions *via* a sawtooth injection current and a constant tuning temperature. A pump-driven water chiller protected the operating laser device. The collimated output of the laser was split into two beams, where one beam was transmitted through the sample gas, focused by a lens, filtered, and then detected by a liquid-nitrogen-cooled InSb detector (Infrared Associates.Inc). The other beam was sent through a silicon etalon (Light-Machinery.Inc), with a free spectral range of 0.018 cm^{-1}. The latter provided a wavelength calibration *via* time domain to wavelength domain transformation in a fifth-order polynomial fit. This indicated that the laser wavelength was tuned over a 2.1 cm^{-1} range at a repetition rate of 100 Hz. All detected signals were acquired by oscilloscopes (DPO3034, Tektronix) and averaged over 200 scan periods to improve the signal-to-noise ratio.

4. Data analysis

The crucial issue for absorption measurements is to obtain an accurate I_0, which was determined by fitting the non-absorbed wing of the background-subtracted transmission I_t with a fifth-order polynomial. The absorption line shape was fitted with a three-peak Voigt function near 2192 cm^{-1} and 2193 cm^{-1}. From these results, the integrated absorbance and collisional width were deduced. Fig. 3 shows an example of the raw signal of the N_2O transitions near 4.56 μm in a gas mixture of 0.42% N_2O/N_2, at $T=298$ K and $P=10$ Torr. The absorption spectrum was calculated from the transmitted signal I_t and the baseline I_0 using Eq. (3), while the time domain was transformed into the wavelength domain using the etalon signal. The absorption line shapes were accurately fitted with three-line Voigt profiles with residuals of less than 1%, as shown in Fig. 3(b). The integrated absorbance A (cm^{-1}) and the collisional Lorentz FWHM $\Delta\nu_c$ (cm^{-1}) of the target transitions were obtained by the multi-peak Voigt fit. Even though the temperature was known, it should be noted that to obtain the true broadening, the multi-peak Voigt fit must be carefully performed because of the convolution of the Gaussian and Lorentzian line shapes.

For line strength measurements, the absorption spectra of N_2O were scanned over the pressure range 2–25 Torr at a fixed temperature. At each temperature and pressure, three measurements were performed and averaged to evaluate

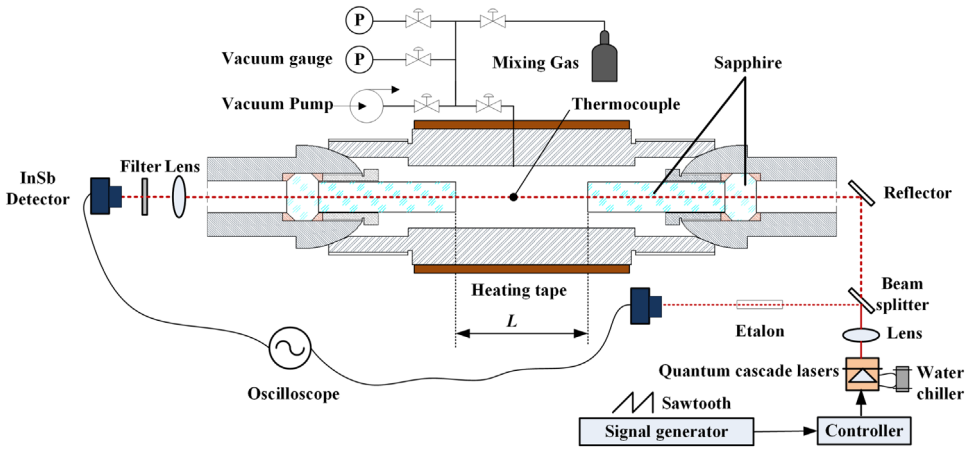

Fig. 2. Schematic of the optical cell for the quantitative measurements of spectral parameters.

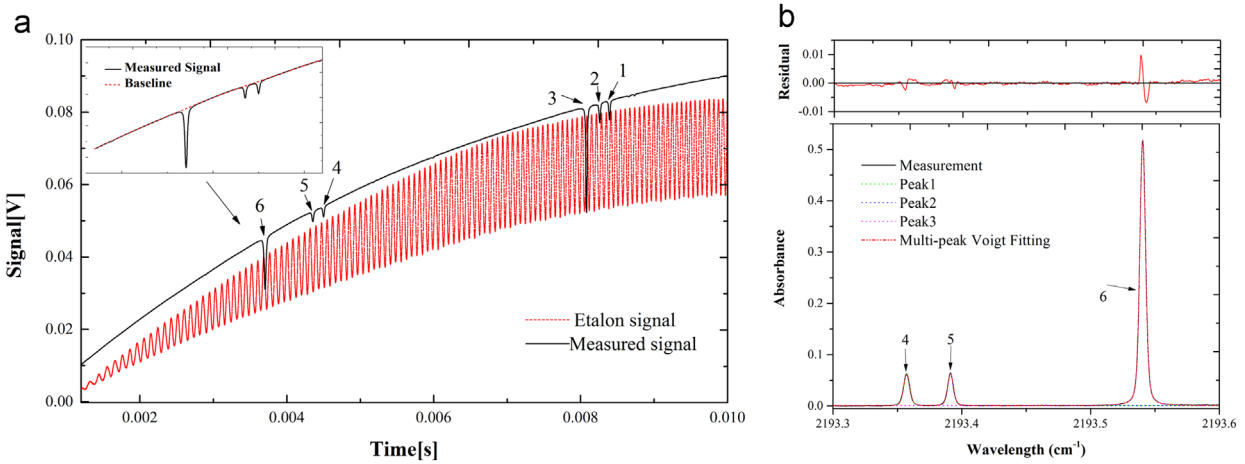

Fig. 3. Example of raw data and analysis, (a) Raw data traces (solid black line: transmission through the cell, dotted red line: transmission through the etalon) at $T=298$ K, $P=10$ Torr and $L=5.86$ cm. The inset shows the polynomial baseline fit (dashed line) for lines 4, 5 and 6; (b) the processed line shape of lines 4, 5 and 6 (solid line), the three-line Voigt fit (dotted red line) and the residual (top panel). (For interpretation of the references to color in this figure legend, the reader is referred to the web version of this article.)

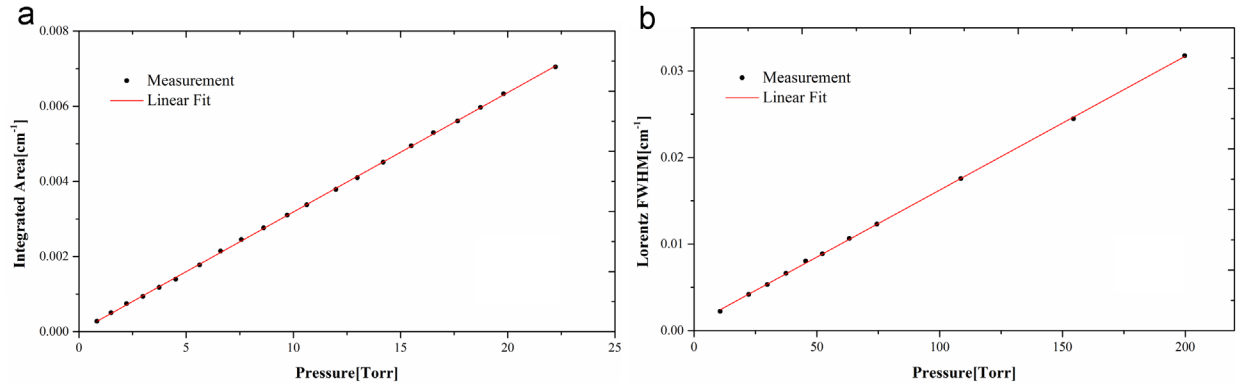

Fig. 4. Determination of line strengths and broadening coefficients at T=298 K for the $P(32)$ transition at 2193.54 cm^{-1} at various pressure. (a) Line strengths derived from the linear fit to the integrated absorbance, $S(298\ K)=9.35\pm0.02$ (cm^{-2} atm^{-1}), (b)N_2-broadening coefficients derived from the linear fit to the collisional FWHM, $\gamma_{N2}(298\ K)=0.0675\pm0.0002$ (cm^{-1} atm^{-1}).

the stability and improve the accuracy and precision. The integrated absorbance over the pressure range was fitted by a linear function, and the line strength $S(T)$ at each temperature was derived from the slope using Eq. (2). The results for the $P(32)$ transition at 2193.54 cm^{-1} are shown in Fig. 4(a). Based on 10 measured line strengths over the

temperature range 298–800 K, the line strength at the reference temperature $S(296\,K)$ was derived from a non-linear fit according to Eq. (3).

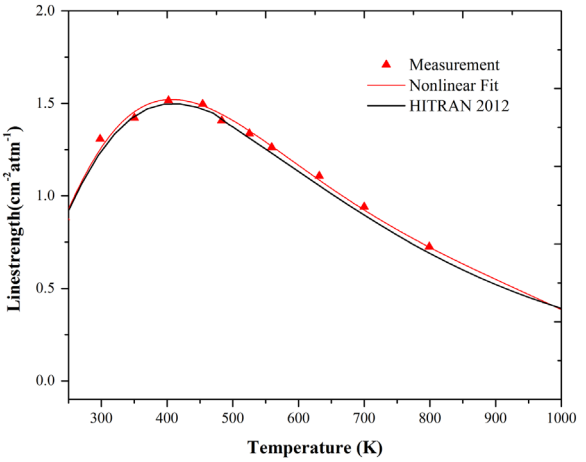

Fig. 5. Measured (red triangles) and HITRAN 2012 (black line) line strengths *vs.* temperature for the *P*(19 f) transition at 2192.40 cm^{-1}. (For interpretation of the references to color in this figure legend, the reader is referred to the web version of this article.)

To obtain broadening coefficients and temperature exponents, similar experiments were performed over the pressure range 10–200 Torr and at 10 temperatures over 298–800 K. The N_2-broadening coefficient γ_{N_2} at a specific temperature was derived from the slope of a linear fit to the measured Lorentzian FWHM as a function of pressure using Eq. (7), as shown in Fig. 4(b). From the 10 N_2-broadening coefficients, the collisional pressure-broadening coefficient at the reference temperature $\gamma_{N_2}(296K)$ and the temperature exponent n were derived by fits according to Eq. (8).

5. Results and discussions

Fig. 5 plots the measured line strengths at 10 temperatures over 298–800 K for the *P*(19f) transition at 2192.40 cm^{-1}. The line strength at the reference temperature $S(296\,K)$ was obtained with an uncertainty of less than 1%. Also plotted are values from the HITRAN 2012 database: the measured line strengths are 1–5% larger at all temperatures. Fig. 6 plots measured line strengths for the six N_2O transitions over the temperature range 298–800 K. Table 2 lists the measured line strengths, as well as corresponding HITRAN 2012 and GEISA 2009 values, at the reference temperature of 296 K. The measured line

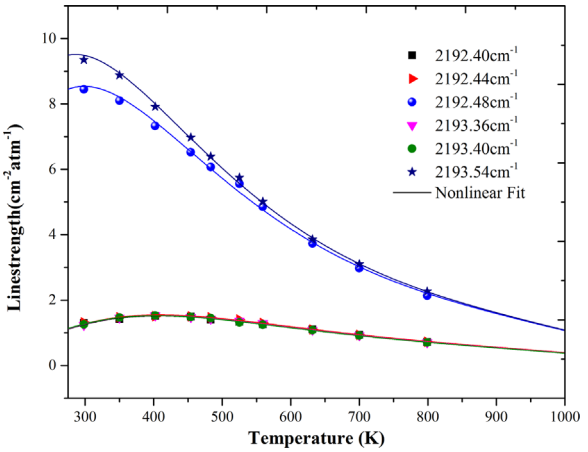

Fig. 6. Measured line strengths (symbols) for six transitions *vs.* temperature and nonlinear fits used to derive the line strengths at the reference temperature S (296 K).

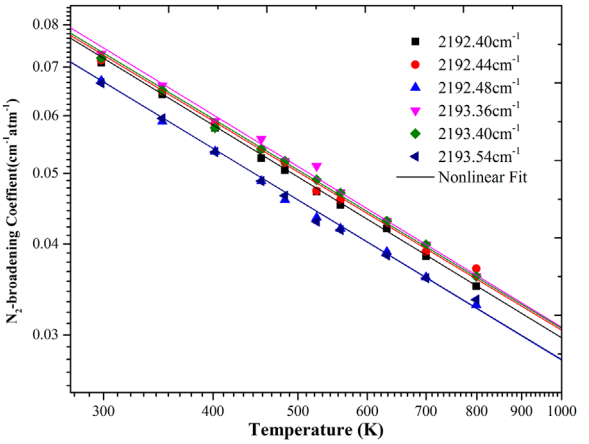

Fig. 7. Measured N_2-broadening coefficients (symbol) *vs.* temperature for six N_2O transitions.

Table 2
Comparison of Line strengths between measurements, HITRAN 2012 and GEISA 2009 databases for six N_2O transitions.

Line	Wavelength (cm^{-1})	Measurements		Hitran 2012		ΔS/ S_{Hitran} %	GEISA 2009	ΔS/ S_{GEISA} %	Essebbar [32]	
		S(296 K) (cm^{-2}atm^{-1})	δ (%)	S(296 K) (cm^{-2}atm^{-1})	δ (%)		S(296 K) (cm^{-2}atm^{-1})		S(296 K) (cm^{-2}atm^{-1})	δ (%)
1	2192.40	1.24	2.87	1.22		1.64	1.26	−1.59	–	–
2	2192.44	1.26	2.80	1.22		2.94	1.26	0	–	–
3	2192.48	8.54	0.96	8.37		2.03	8.45	1.07	8.40	9.80
4	2193.36	1.25	2.66	1.25	2–5	0	1.29	−3.10	–	–
5	2193.40	1.26	2.62	1.25		0.80	1.29	−2.33	–	–
6	2193.54	9.50	0.81	9.29		2.26	9.38	1.28	9.30	9.62

Table 3
Comparison between measured N_2-broadening coefficients and HITRAN 2012 air-broadening coefficients of the six N_2O transitions.

Line	Wavelength (cm^{-1})	Measurements				Hitran 2012				Essebbar [32]		Difference	
		γ_{N2}(296 K) (cm-1atm-1)	δ (%)	n	δ (%)	γ_{air}(296 K) (cm-1atm-1)	Δ (%)	n_{air}	δ (%)	γ_{N2}(297 K) (cm-1atm-1)	δ (%)	$\Delta\gamma/\gamma_{HITRAN}$ (%)	$\Delta n/n_{HITRAN}$(%)
1	2192.40	0.0718	2.52	0.721	0.96	0.0754		0.75		–	–	−4.77	−3.87
2	2192.44	0.0721	4.23	0.634	1.52	0.0754		0.75		–	–	−4.37	−15.46
3	2192.48	0.0685	4.38	0.715	1.61	0.0705		0.75		0.0733	1.64	−2.84	−4.67
4	2193.36	0.0743	4.99	0.715	2.53	0.0761	2–5	0.75	5–10	–	–	−2.37	−4.67
5	2193.40	0.0735	4.97	0.702	3.65	0.0761		0.75		–	–	−3.42	−6.4
6	2193.54	0.0683	4.43	0.604	2.56	0.0707		0.75		0.0736	1.77	−3.39	−19.47

strengths at the reference temperature for all lines of interest are 0–3% larger than the HITRAN 2012 values, while the GEISA 2009 values are within ±3.1%. The uncertainty δ for the measurements in Table 2 is the ratio of standard error and measured value derived from the nonlinear fit to the measured data. The uncertainties of the measurements derive from uncertainties in temperature (1%), pressure measurements (0.12%), gas mixture concentrations (0.5%), optical path length determination (1%), and fit error when determining the baseline and lineshape fits (1%).

Fig. 7 plots the measured N_2-broadening coefficients *vs.* temperatures (298–800 K) for the six transitions. The N_2O concentration in the gas mixture was 0.42%; thus there was a negligible contribution of self-broadening effect to the total collisional Lorentz width. The collisional pressure-broadening coefficients at the reference temperature $\gamma_{N_2}(296K)$ and the temperature exponents n were obtained by fitting the data. The measured spectral parameters for the six lines are summarized in Table 3, along with air-broadening coefficients and temperature exponents from the HITRAN 2012 database. As can be seen, the measured N_2-broadening coefficients at the reference temperature of 296 K are 2–5% smaller than the HITRAN 2012 air-broadening coefficients.

6. Summary

Spectral parameters of N_2O transitions near 4.56 μm were measured using a quantum cascade laser. From this data, line strengths, N_2-broadening coefficients, and temperature exponents were determined. Two strong transitions ($P(33)$ and $P(32)$) near 2192.48 cm^{-1} and 2193.54 cm^{-1}, and four weak neighboring transitions, were investigated over the temperature range 298–800 K and the pressure range 2–200 Torr. A comparison with the HITRAN 2012 database indicates that the measured line strengths at the reference temperature of 296 K for all lines of interest were 0–3% larger. Meanwhile the N_2-broadening coefficients at the same reference temperature were 2–5% smaller than the HITRAN 2012 air-broadening coefficients.

Acknowledgments

This work was sponsored by the National Natural Science Foundation of China (Grant nos. 11372329 and 90816015).

References

[1] Chao X, Jeffries JB, Hanson RK. In situ absorption sensor for NO in combustion gases with a 5.2 mu m quantum-cascade laser. Proc Combust Inst 2011;33:725–33.
[2] Schultz IA, et al. Multispecies midinfrared absorption measurements in a hydrocarbon-fueled scramjet combustor. J Propuls Power 2014;30(6):1595–604.
[3] Spearrin R, et al. Simultaneous sensing of temperature, CO, and CO_2 in a scramjet combustor using quantum cascade laser absorption spectroscopy. Appl Phys B 2014;117(2):689–98.
[4] Ren W. Mid-infrared laser diagnostics for chemical kinetics study of oxygenates [PhD thesis]. Stanford University, High Temperature Gas dynamics Laboratory. Stanford, CA: Mechanical Engineering Department; 94305, 2013.
[5] Zeng H, et al. Midinfrared absorption measurements of nitrous oxide in ammonium dinitramide monopropellant thruster. J Propuls Power 2015:1–5.
[6] Rothman L, et al. The HITRAN2012 molecular spectroscopic database. J Quant Spectrosc Radiat Transf 2013;130:4–50.
[7] Jacquinet-Husson N, et al. The 2009 edition of the GEISA spectroscopic database. J Quant Spectrosc Radiat Transf 2011;112(15):2395–445.
[8] Liu X, Jeffries JB, Hanson RK. Measurements of spectral parameters of water-vapour transitions near 1388 and 1345 nm for accurate simulation of high-pressure absorption spectra. Meas Sci Technol 2007;18(5):1185.
[9] Li H, et al. Diode laser measurements of temperature-dependent collisional-narrowing and broadening parameters of Ar-perturbed H_2O transitions at 1391.7 and 1397.8 nm. J Quant Spectrosc Radiat Transf 2008;109(1):132–43.
[10] Liu X, et al. Experimental study of H_2O spectroscopic parameters in the near-IR (6940–7440 $cm(^{-1})$) for gas sensing applications at elevated temperature. J Quant Spectrosc Radiat Transf 2007;103(3):565–77.
[11] Goldenstein CS, Hanson RK. Diode-laser measurements of linestrength and temperature-dependent lineshape parameters for H2O transitions near 1.4 mu m using Voigt, Rautian, Galatry, and speed-dependent Voigt profiles. J Quant Spectrosc Radiat Transf 2015;152:127–39.
[12] US Environmental Protection Agency. Global Greenhouse Gas Emissions Data. 2015; Available from: ⟨http://www3.epa.gov/climatechange/ghgemissions/global.html⟩.
[13] Zakirov V, et al. Nitrous oxide as a rocket propellant. Acta Astronaut 2001;48(5):353–62.
[14] Zakirov V, et al. Nitrous oxide as a rocket propellant for small satellites. In: Proceedings of the 5th International Symposium on Small Satellite Systems and Services, France; 2000.
[15] Lohner K, et al. Design and development of a sub-scale nitrous oxide monopropellant gas generator. AIAA Pap. 2007;5463:8–11.

[16] Lohner K, et al. Nitrous Oxide Monopropellant Gas Generator Development. in 3rd Spacecraft Propulsion Joint Subcommittee Meeting, JANNAF; 2008.
[17] Wallbank J, et al. Nitrous oxide as a green monopropellant for small satellites. in ESA Special Publication; 2004.
[18] Toth RA. Line strengths (900–3600 cm($^{-1}$)), self-broadened linewidths, and frequency shifts (1800–2360 cm($^{-1}$)) of N($_2$)O. Appl Opt 1993;32(36):7326–65.
[19] Toth RA. Line strengths of N_2O in the 1120–1440-cm^{-1} region. Appl Opt 1984;23(11):1825–34.
[20] Toth RA. N_2O vibration–rotation parameters derived from measurements in the 900–1090-and 1580–2380-cm − 1 regions. JOSA B 1987;**4**(3):357–74.
[21] Toth RA. N^{2-} and air-broadened linewidths and frequency-shifts of N_2O. J Quant Spectrosc Radiat Transf 2000;66(3):285–304.
[22] Daumont L, et al. Line intensities of: the 10 μm region revisited. J Quant Spectrosc Radiat Transf 2002;72(1):37–55.
[23] Daumont L, et al. Line intensity measurements in 14N216O and their treatment using the effective dipole moment approach. J Mol Spectrosc 2001;208(2):281–91.
[24] Daumont L, et al. Line intensity measurements in 14N216O and their treatment using the effective dipole moment approach.II. The 5400–11000 cm^{-1} region. J Quant Spectrosc Radiat Transf 2007;104(3):342–56.
[25] Rachet F, et al. Linestrength Measurements for N_2O Around 4 μm: $\Pi \leftarrow \Sigma$, $\Pi \leftarrow \Pi$, $\Sigma \leftarrow \Pi$, and $\Delta \leftarrow \Pi$ Transitions in 14N216O (2400–2850 cm^{-1}). J Mol Spectrosc 1994;164(1):196–209.
[26] Elazizi M, et al. Linestrength Measurements for N_2O around 4 μm: $\Sigma \leftarrow \Sigma$ Transitions in Four Isotopic Species (2400–2600 cm^{-1}). J Mol Spectrosc 1994;164(1):180–95.
[27] Regalia L, et al. Intensities of N_2O measurements in the 4 and 3 μm region using fourier transform spectrometer. J Quant Spectrosc Radiat Transf 1997;57(4):435–44.
[28] Nemtchinov V, Sun C, Varanasi P. Measurements of line intensities and line widths in the ν3-fundamental band of nitrous oxide at atmospheric temperatures. J Quant Spectrosc Radiat Transf 2004;83(3–4):267–84.
[29] Lacome N, Levy A, Guelachvili G. Fourier transform measurement of self-, N($_2$)-, and O($_2$)-broadening of N($_2$)O lines: temperature dependence of linewidths. Appl Opt 1984;23(3):425–35.
[30] Tang L-W, Nadler S, Daunt SJ. Tunable diode laser measurements of absolute line strengths in the 2v2 band of N_2O near 8 μm. J Quant Spectrosc Radiat Transf 1989;41(2):97–101.
[31] Loewenstein M, et al. Diode laser measurements of line strengths and widths in the 4.5-μm bands of N_2O. J Quant Spectrosc Radiat Transf 1986;35(3):231–5.
[32] Es-Sebbar ET, Deli M, Farooq A. Quantum cascade laser measurements of line intensities, N2-, O2- and Ar- collisional broadening coefficients of N2O in the nu3 band near 4.5 micron. Appl Spectrosc 2016;70(6):972–82.
[33] Goldenstein CS, Jeffries JB, Hanson RK. Diode laser measurements of linestrength and temperature-dependent lineshape parameters of H 2 O-, CO 2-, and N 2-perturbed H 2 O transitions near 2474 and 2482 nm. J Quant Spectrosc Radiat Transf 2013;130:100–11.
[34] Rieker G.B., Wavelength-modulation spectroscopy for measurements of gas temperature and concentration in harsh environment [PhD thesis], Stanford University, High Temperature Gas dynamics Laboratory. Stanford, CA; Mechanical Engineering Department; 94305, 2009.
[35] Rice S, et al. Design strategies for optically-accessible, high-temperature, high-pressure reactor cells. Sandia Report SAND99-8260; 2000.
[36] Space Propulsion Group, Inc. Nitrous Oxide Safety; 2012. Available from: ⟨http://www.spg-corp.com/nitrous-oxide-safety.html⟩.